

# Conditional Denoising Diffusion Probabilistic Models for Data Reconstruction Enhancement in Wireless Communications

Mehdi Letafati, *Student Member, IEEE*, Samad Ali, *Member, IEEE*, and Matti Latva-aho, *Fellow, IEEE*

**Abstract**—In this paper, conditional denoising diffusion probabilistic models (CDiffs) are proposed to enhance the data transmission and reconstruction over wireless channels. The underlying mechanism of diffusion models is to decompose the data generation process over the so-called “denoising” steps. Inspired by this, the key idea is to leverage the generative prior of diffusion models in learning a “noisy-to-clean” transformation of the information signal to help enhance data reconstruction. The proposed scheme could be beneficial for communication scenarios in which a prior knowledge of the information content is available, e.g., in multimedia transmission. Hence, instead of employing complicated channel codes that reduce the information rate, one can exploit diffusion priors for reliable data reconstruction, especially under extreme channel conditions due to low signal-to-noise ratio (SNR), or hardware-impaired communications. The proposed CDiff-assisted receiver is tailored for the scenario of wireless image transmission using MNIST dataset. Our numerical results highlight the reconstruction performance of our scheme compared to the conventional digital communication, as well as the deep neural network (DNN)-based benchmark. It is also shown that more than 10 dB improvement in the reconstruction could be achieved in low SNR regimes, without the need to reduce the information rate for error correction.

**Index Terms**—AI-native wireless, diffusion priors, generative AI, wireless AI, conditional denoising diffusion models, reliable communication.

## I. INTRODUCTION

### A. Motivation & Background

With the emergence of deep generative models, the realm of artificial intelligence (AI) has witnessed a paradigm shift towards the novel concept of generative AI that can facilitate the development of AI-based systems [2]–[4]. At the same time, from data communication and networking perspective, “connected intelligence” is envisioned as the most significant driving force in the sixth generation (6G) of communications—AI and machine learning (AI/ML) algorithms are envisioned to be widely incorporated into 6G wireless networks, realizing “AI-native” communication systems [5]–[8]. This underscores the need for novel AI/ML-based solutions to be tailored to meet the requirements of emerging communication scenarios.

The evolution of diffusion models [9], as the new paradigm in deep generative models, can be regarded as one of the main

factors contributing to the recent breakthroughs in generative AI, that have already showcased notable success with some of the popular examples such as DALL.E 2 by OpenAI,<sup>1</sup> and ImageGen by Google Brain.<sup>2</sup> Diffusion models have realized unprecedented results in different applications, such as computer vision, natural language processing (NLP), data analysis and synthesis, and medical imaging [10]. Please see [11] and references therein for a comprehensive survey on diffusion models. The core concept of diffusion modeling is that if we could develop an ML model that is capable of learning the *systematic decay of information*, due to noise/distortions, then it should be possible to “reverse” the process and recover the information back from the noisy/erroneous data. This is fundamentally different from conventional generative models, like generative adversarial networks (GANs) and variational autoencoders (VAEs). Accordingly, the close underlying relation between the key concepts on how diffusion models work and the problems in wireless communication systems has motivated us to carry out this research.

### B. Related Works

Ongoing research on diffusion models encompasses both theoretical advancements and practical applications across different domains of computer science [11]. However, there have been only a few papers in wireless communication literature that have started looking into the potential merits of diffusion-based generative models for wireless systems [3], [4], [12]–[17]. The authors in [12] study a workflow for utilizing diffusion models in wireless network management. They study the incentive mechanisms for generating contracts using diffusion models in mobile AI-generated content services. They exploit the exploration capability of diffusion models in Q-learning algorithms for network management. Denoising diffusion model is utilized in [13] to generate synthetic channel realizations conditioned on the message information. The authors tackle the problem of differentiable channel model within the gradient-based training process of end-to-end ML-based communications. The results highlight the performance of diffusion models as an alternative to GAN-based schemes. It is shown in [13] that GANs experience unstable training and less diversity in generation performance, due to their adversarial training nature. However, diffusion models maintain a more stable training process and a better generalization

Preliminary results of this paper were presented at the IEEE Wireless Communications and Networking Conference (WCNC 2024), Dubai, United Arab Emirates, Apr. 2024 [1].

The authors are with the Centre for Wireless Communications, University of Oulu, Oulu, Finland (e-mails: mehdi.letafati@oulu.fi; samad.ali@oulu.fi; matti.latva-aho@oulu.fi).

<sup>1</sup><https://openai.com/dall-e-2>

<sup>2</sup><https://imagen.research.google/>

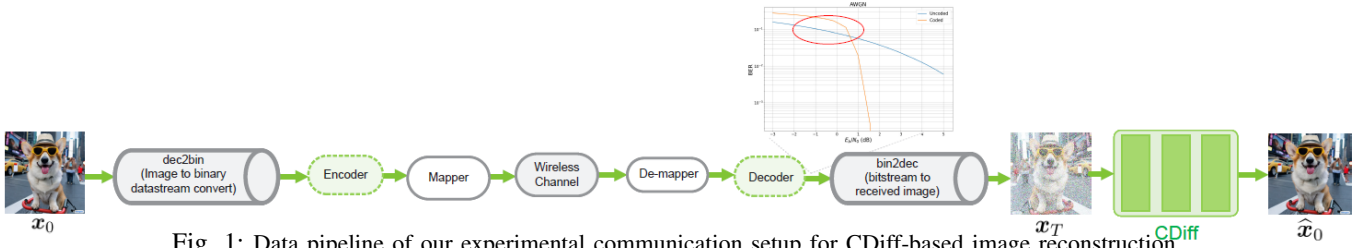


Fig. 1: Data pipeline of our experimental communication setup for CDiff-based image reconstruction.

during inference. Noise-conditioned score network (NCSN)-based channel estimation is studied in [14] and [15] for multi-input-multi-output (MIMO) wireless communication scenario. The authors estimate the gradient of the high-dimensional log-prior of wireless channels, using RefineNet neural network architecture. Posterior sampling method is further applied to make the generated channel estimations consistent with the pilot signals measured at the receiver. Diffusion models have also been incorporated into the so-called semantic communication systems in [16], [17]. More specifically, deep learning-based joint source-channel coding (Deep-JSCC) is combined with diffusion models to complement semantic data transmission schemes with a generative component. The initial results show that the perceptual quality of reconstruction can be improved in such scenarios. Nevertheless, those schemes in [16], [17] propose to employ two different types of deep learning models each maintaining a distinct objective function (while their optimization also depends on each other), i.e., the autoencoder for semantic transmission and reception, and the diffusion models for reconstruction enhancement. This can impose serious concerns in terms of the computational overhead to the network. In addition, the output signal of a neural encoder (i.e., the channel input) does not necessarily follow the standard format of modulation signals, which makes it challenging to employ semantic transmission ideas in a real-world communication scenario.

### C. Our Contributions

In this paper, we propose conditional denoising diffusion probabilistic models (DDPM) for enhancing the wireless image transmission in digital communication schemes. Different from GANs and VAEs, the underlying mechanism of diffusion models is to first transform the ground-truth signal into an isotropic Gaussian distribution in the forward diffusion process, and then try to regenerate data over the so-called “denoising” steps by removing the noise introduced in the diffusion process. DDPMs in their vanilla format are based upon the assumption that the denoising process starts with isotropic Gaussian noise [9]. However, in a practical wireless system, the received/decoded signals are a degraded version of the ground-truth information signals, not necessarily a pure isotropic Gaussian noise, while the degradation is different in different distortion conditions such as different SNRs and transceiver specifications. To address this, we propose conditional diffusion models (CDiff), in which the noisy degraded signals are incorporated into the denoising framework of the diffusion model. This way, the diffusion model learns to

reconstruct the ground-truth information from the degraded received signal, instead of a pure noise.

In our scheme, the generative prior of conditioned DDPMs is exploited to enhance data reconstruction at the receiver of a communication system. This is particularly pronounced in extreme channel conditions with poor connectivity due to low signal-to-noise ratio (SNR), or hardware-impaired communications. In such scenarios, error correcting codes might not be able to correct the mismatches, or complicated codes might be needed at the cost of decreasing the information rate to correct the errors. Instead, the proposed diffusion-aided scheme can be utilized for reliable data reconstruction without the need for decreasing the information rate. This can be tailored for the communication scenarios, in which a prior knowledge of the information signals is available that can be exploited by a DDPM to learn the “denoising” process. Our scheme is not simply a direct application of the seminal papers in diffusion model research. We do not directly apply the seminal DDPM paper [9] into a communication system. Rather, different from [9], we incorporate the wireless “conditions” into the diffusion model via employing a *wireless CDiff*.

The proposed DDPM-assisted receiver is employed in conjunction with the NVIDIA Sionna simulator<sup>3</sup>, by plugging the trained diffusion model to the receiver side. Data communication pipeline of our scheme is shown in Fig. 1, which highlights the compatibility of the scheme with a practical communication system. Moreover, in contrast to [16], [17], the proposed scheme does not rely on any additional autoencoder model. Numerical results highlight that the *robustness* of the wireless system can be improved against practical non-idealities such as hardware impairments and channel distortions. We compare the reconstruction performance of our scheme to the conventional digital communications without diffusions, and also the deep neural network (DNN)-based benchmark [18]. It is also shown that more than 10 dB improvement in the reconstruction could be achieved in low SNR regimes, without the need to reduce the information rate for error correction.

### D. Paper Organization and Notations

The rest of the paper is organized as follows. In Section II, we first introduce the concept of DDPMs, the forward, and the reverse diffusion processes, together with the main formulas and the corresponding loss functions. We also try to point out insightful intuitions behind the main formulas of the DDPM

<sup>3</sup><https://github.com/NVlabs/sionna>

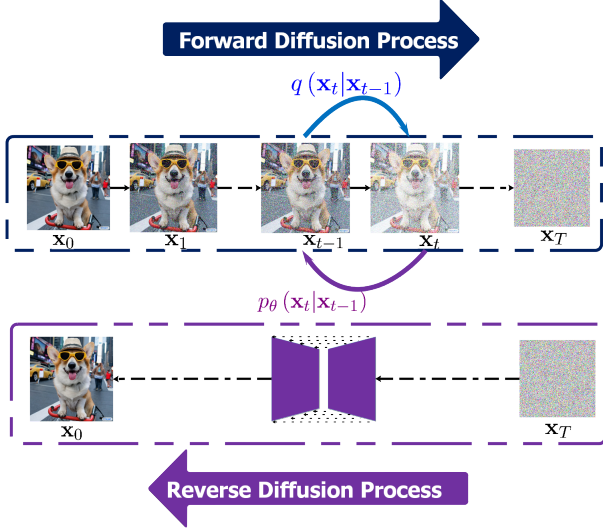


Fig. 2: Diffusion models: A general overview. A Markov chain is defined to mimic the forward diffusion steps, during which random perturbation noise is purposefully added to the original data. Then in a reverse process, the model learns to construct the desired data samples out of noise.

framework. Our system model is introduced in Section III. We first provide the generic formulation of a communication system under RF impairments. We then address the proposed conditional DDPM by modifying the vanilla diffusion model. Numerical experiments are provided in Section IV. Finally, Section V concludes the paper.

*Notations:* Vectors and matrices are represented, respectively, by bold lower-case and upper-case symbols. Absolute value of a scalar variable and the  $\ell_2$  norm of a vector are denoted, respectively, by  $|\cdot|$  and  $\|\cdot\|$ . Notation  $\mathcal{N}(\mathbf{x}; \boldsymbol{\mu}, \boldsymbol{\Sigma})$  stands for the multivariate normal distribution with mean vector  $\boldsymbol{\mu}$  and covariance matrix  $\boldsymbol{\Sigma}$  for a random vector  $\mathbf{x}$ . Similarly, complex normal distribution with the corresponding mean vector and covariance matrix is denoted by  $\mathcal{CN}(\boldsymbol{\mu}, \boldsymbol{\Sigma})$ . Moreover, the expected value of a random variable is denoted by  $\mathbb{E}[\cdot]$ . Sets are denoted by calligraphic symbols, and  $\mathbf{0}$  and  $\mathbf{I}$  show all-zero vector and identity matrix of the corresponding size, respectively. Moreover,  $[N]$ , (with  $N$  as integer) denotes the set of all integer values from 1 to  $N$ , and  $\text{Unif}[N]$ ,  $N > 1$ , denotes discrete uniform distribution with samples between 1 to  $N$ . Real and imaginary parts of a complex-valued vector are denoted by  $\Re\{\cdot\}$  and  $\Im\{\cdot\}$ , respectively.

## II. INVESTIGATION OF DENOISING DIFFUSION PROBABILISTIC MODELS

In this section, we provide insights into the underlying mechanisms of the DDPM model. We also provide a comprehensive overview of the theoretical foundations and practical implications of the DDPM model, offering a deeper understanding of its potential impact on communication systems.

### A. Theoretical Foundations

Diffusion models are comprised of two processes, namely the forward diffusion process and the parametric reverse diffusion process, as illustrated in Fig. 2. During the forward process, samples are diffused using Gaussian kernels to add noise until the fully-distorted signals follow an isotropic Gaussian distribution. Then in the reverse process, the model tries to “decode” the data via “denoising” the perturbed samples in a hierarchical fashion.

1) *Forward Diffusion Process:* Let  $\mathbf{x}_0$  be a data sample from some distribution  $q(\mathbf{x}_0)$ , i.e.,  $\mathbf{x}_0 \sim q(\mathbf{x}_0)$ . For a finite number,  $T$ , of time-steps, the forward diffusion process  $q(\mathbf{x}_t|\mathbf{x}_{t-1})$  is defined by adding Gaussian noise at each time-step  $t \in [T]$  according to a known “variance schedule”  $0 < \beta_1 < \dots < \beta_T < 1$ . This is formulated as

$$q(\mathbf{x}_t|\mathbf{x}_{t-1}) \sim \mathcal{N}(\mathbf{x}_t; \sqrt{1 - \beta_t}\mathbf{x}_{t-1}, \beta_t\mathbf{I}), \quad (1)$$

$$q(\mathbf{x}_{1:T}|\mathbf{x}_0) = \prod_{t=1}^T q(\mathbf{x}_t|\mathbf{x}_{t-1}). \quad (2)$$

Invoking (2), the data sample gradually loses its distinguishable features as the time-step goes on, where with  $T \rightarrow \infty$ ,  $\mathbf{x}_T$  approaches an isotropic Gaussian distribution. According to (1), each new sample at time-step  $t$  can be drawn from a conditional Gaussian distribution with mean vector  $\boldsymbol{\mu}_t = \sqrt{1 - \beta_t}\mathbf{x}_{t-1}$  and covariance matrix  $\boldsymbol{\Sigma}_t^2 = \beta_t\mathbf{I}$ . Hence, the forward process is realized by sampling from a Gaussian noise  $\boldsymbol{\epsilon}_{t-1} \sim \mathcal{N}(\mathbf{0}, \mathbf{I})$  and setting

$$\mathbf{x}_t = \sqrt{1 - \beta_t}\mathbf{x}_{t-1} + \sqrt{\beta_t}\boldsymbol{\epsilon}_{t-1}. \quad (3)$$

By recursively applying the reparameterization trick from ML literature [20], we can sample  $\mathbf{x}_t$  at any arbitrary time-step  $t$  in a closed-form expression. This results in

$$\mathbf{x}_t = \sqrt{\bar{\alpha}_t}\mathbf{x}_0 + \sqrt{1 - \bar{\alpha}_t}\boldsymbol{\epsilon}_0, \quad (4)$$

$$q(\mathbf{x}_t|\mathbf{x}_0) \sim \mathcal{N}(\mathbf{x}_t; \sqrt{\bar{\alpha}_t}\mathbf{x}_0, (1 - \bar{\alpha}_t)\mathbf{I}), \quad (5)$$

where  $\bar{\alpha}_t = \prod_{i=1}^t (1 - \alpha_i)$  and  $\alpha_t = 1 - \beta_t$ . Note that (4) implies that we can directly sample  $\mathbf{x}_t$  from  $\mathbf{x}_0$  for all  $t \in [T]$ .

2) *Parametric Reverse Diffusion Process:* Now the problem is to reverse the process in (4) and sample from  $q(\mathbf{x}_{t-1}|\mathbf{x}_t)$ , so that we regenerate the true samples from some Gaussian noise  $\mathbf{x}_T$ . However, we cannot easily estimate the distribution, since it requires knowing the distribution of all possible data samples (or equivalently exploiting the entire dataset). Hence, to approximate the conditional probabilities and run the reverse diffusion process, we need to learn a probabilistic model  $p_\theta(\mathbf{x}_{t-1}|\mathbf{x}_t)$  that is parameterized by  $\theta$ . Accordingly, the following expressions can be written

$$p_\theta(\mathbf{x}_{t-1}|\mathbf{x}_t) \sim \mathcal{N}(\mathbf{x}_{t-1}; \boldsymbol{\mu}_\theta(\mathbf{x}_t, t), \boldsymbol{\Sigma}_\theta(\mathbf{x}_t, t)). \quad (6)$$

Now the problem simplifies to learning the mean vector  $\boldsymbol{\mu}_\theta(\mathbf{x}_t, t)$  and the covariance matrix  $\boldsymbol{\Sigma}_\theta(\mathbf{x}_t, t)$  for the probabilistic model  $p_\theta(\cdot)$ , where a neural network (parameterized by  $\theta$ ) can be trained to approximate (learn) the reverse process. When we have  $\mathbf{x}_0$  as a reference, we can take a small step backwards from noise to generate the data samples, and the reverse step would be formulated as  $q(\mathbf{x}_{t-1}|\mathbf{x}_t, \mathbf{x}_0)$ .

Mathematically speaking, by knowing the conditional probabilities of  $q(\mathbf{x}_t|\mathbf{x}_0)$  and  $q(\mathbf{x}_{t-1}|\mathbf{x}_0)$ , and utilizing Bayes rule, we can derive  $q(\mathbf{x}_{t-1}|\mathbf{x}_t, \mathbf{x}_0)$  with a similar expression to (6):

$$q(\mathbf{x}_{t-1}|\mathbf{x}_t, \mathbf{x}_0) \sim \mathcal{N}(\mathbf{x}_{t-1}; \tilde{\boldsymbol{\mu}}(\mathbf{x}_t, \mathbf{x}_0, t), \tilde{\boldsymbol{\beta}}_t \mathbf{I}), \quad (7)$$

$$\tilde{\boldsymbol{\mu}}(\mathbf{x}_t, \mathbf{x}_0, t) = \frac{\sqrt{\bar{\alpha}_t}(1 - \bar{\alpha}_{t-1})}{1 - \bar{\alpha}_t} \mathbf{x}_t + \frac{\sqrt{\bar{\alpha}_{t-1}}\beta_t}{1 - \bar{\alpha}_t} \mathbf{x}_0, \quad (8)$$

$$\tilde{\boldsymbol{\beta}}_t = \frac{1 - \bar{\alpha}_{t-1}}{1 - \bar{\alpha}_t} \beta_t. \quad (9)$$

Invoking (9), one can infer that the covariance matrix has no learnable parameter. Hence, we simply need to learn the mean vector  $\tilde{\boldsymbol{\mu}}(\mathbf{x}_t, \mathbf{x}_0, t)$ . Using the reparameterization trick and with a similar approach to (4), we can express  $\mathbf{x}_0$  as

$$\mathbf{x}_0 = \frac{1}{\sqrt{\bar{\alpha}_t}} (\mathbf{x}_t - \sqrt{1 - \bar{\alpha}_t} \boldsymbol{\epsilon}_t). \quad (10)$$

Substituting  $\mathbf{x}_0$  in (8) by (10) results in

$$\tilde{\boldsymbol{\mu}}(\mathbf{x}_t, \mathbf{x}_0, t) = \frac{1}{\sqrt{\bar{\alpha}_t}} \left( \mathbf{x}_t - \frac{1 - \alpha_t}{\sqrt{1 - \bar{\alpha}_t}} \boldsymbol{\epsilon}_t \right). \quad (11)$$

Now we can learn the conditioned probability distribution  $p_{\theta}(\mathbf{x}_{t-1}|\mathbf{x}_t)$  of the reverse diffusion process by training a neural network that approximates  $\tilde{\boldsymbol{\mu}}(\mathbf{x}_t, \mathbf{x}_0, t)$ . Therefore, we simply need to set the approximated mean vector  $\boldsymbol{\mu}_{\theta}(\mathbf{x}_t, t)$  to have the same mathematical format as the target mean vector  $\tilde{\boldsymbol{\mu}}(\mathbf{x}_t, \mathbf{x}_0, t)$ . Hence we have

$$\boldsymbol{\mu}_{\theta}(\mathbf{x}_t, t) = \frac{1}{\sqrt{\bar{\alpha}_t}} \left( \mathbf{x}_t - \frac{1 - \alpha_t}{\sqrt{1 - \bar{\alpha}_t}} \boldsymbol{\epsilon}_{\theta}(\mathbf{x}_t, t) \right), \quad (12)$$

where  $\boldsymbol{\epsilon}_{\theta}(\mathbf{x}_t, t)$  denotes the model to predict  $\boldsymbol{\epsilon}_t$ .

We now define the loss function  $\mathcal{L}_t$  for time-step  $t$ , aiming to minimize the difference between  $\boldsymbol{\mu}_{\theta}(\mathbf{x}_t, t)$  and  $\tilde{\boldsymbol{\mu}}(\mathbf{x}_t, \mathbf{x}_0, t)$ .

$$\begin{aligned} \mathcal{L}_t &= \mathbb{E}_{\substack{t \sim \text{Unif}[T] \\ \mathbf{x}_0 \sim q(\mathbf{x}_0) \\ \boldsymbol{\epsilon}_0 \sim \mathcal{N}(0, \mathbf{I})}} \left[ \|\boldsymbol{\epsilon}_t - \boldsymbol{\epsilon}_{\theta}(\mathbf{x}_t, t)\|^2 \right] \\ &= \mathbb{E}_{\substack{t \sim \text{Unif}[T] \\ \mathbf{x}_0 \sim q(\mathbf{x}_0) \\ \boldsymbol{\epsilon}_0 \sim \mathcal{N}(0, \mathbf{I})}} \left[ \|\boldsymbol{\epsilon}_t - \boldsymbol{\epsilon}_{\theta}(\sqrt{\bar{\alpha}_t} \mathbf{x}_0 + \sqrt{1 - \bar{\alpha}_t} \boldsymbol{\epsilon}_t, t)\|^2 \right]. \end{aligned} \quad (13)$$

Invoking (13), at each time-step  $t$ , the DDPM model takes  $\mathbf{x}_t$  as input and returns the distortion components  $\boldsymbol{\epsilon}_{\theta}(\mathbf{x}_t, t)$ . Moreover,  $\boldsymbol{\epsilon}_t$  denotes the diffused noise term at time-step  $t$ .

### B. Practical Implications and Potential Impacts on Communication Systems

As discussed above, DDPMs are inherently connected to the task of *denoising*. This makes them highly relevant to communication systems, where the unwanted noise and interference is a significant challenge. This implies some of the potential impacts of DDPMs on communication systems. Notably, DDPMs as powerful denoising models can be applied to clean noisy signals received over communication channels. The reverse diffusion process could help reconstruct original signals from noisy transmissions, leading to improved signal quality [4]. Further, DDPMs could be integrated into an end-to-end framework, where both the transmitter and

receiver are learned jointly. The transmitter could use a forward diffusion process to generate noisy encoding of the transmitted signal, while the receiver could use the reverse process to decode the original data, optimizing the overall communication pipeline for robustness and efficiency [13].

To conclude, we note that theoretical robustness and practical applications of DDPMs, introduced in this section, highlight that they have the potential to play important roles in future communication systems. This can include, but is not limited to, *resilient communications*, making communication systems more resilient to noise, interference, and distortions, particularly in extreme environments, such as space (non-terrestrial networks), underwater, or urban areas with heavy interference. High-fidelity signal reconstruction is another direct impact of employing DDPMs for communication networks, which can potentially result in clearer voice calls, sharper video transmissions, and more accurate data recovery in practical communication applications.

## III. SYSTEM MODEL AND PROPOSED SCHEME

### A. System Model & Formulas

Consider a point-to-point communication system, where a source node (the transmitter) aims to transmit the ground-truth information  $x_0 \sim q(x_0)$  to a destination node (the receiver) over the communication channel. We denote by  $s$ , the channel input signal subject to the power constraint  $\mathbb{E}[|s|^2] \leq P$ , for which we can write  $s = g(x_0)$  with  $g(\cdot)$  denoting the mapping from information signals to the channel input (including the off-the-shelf modulation and coding functionalities). The information-bearing signal  $s$  is then sent over the communication channel and  $y = \eta(s)$  is observed at the receiver, where  $\eta(\cdot)$  stands for the channel distortion and noise, as well as the impairments caused by the non-ideal transceiver hardware. To model  $\eta(\cdot)$ , we consider a practical scenario of hardware-impaired communication, where we employ the well-known generic communication model of [21]. Denoting the Rayleigh fading wireless channel coefficient by  $h$ , we have

$$y = h(\sqrt{P}s + \tau^t) + \tau^r + n, \quad (14)$$

$$\tau^t \sim \mathcal{CN}(0, \kappa^t P), \quad \tau^r \sim \mathcal{CN}(0, \kappa^r P |h|^2), \quad (15)$$

where  $P$  denotes the transmit power,  $\tau^t$  is the distortion noise caused by the transmitter hardware with the corresponding impairment level  $\kappa^t$ , and  $\tau^r$  reflects the hardware distortion at the receiver with  $\kappa^r$  showing the level of impairment at the receiver hardware. Notably,  $\tau^r$  is conditionally Gaussian, given the channel realization  $h$ . This is a well-known and experimentally-validated model for HIs, which is widely-adopted in wireless communication literature [21]. We emphasize that according to [21], the distortion noise caused at each radio frequency (RF) device is proportional to its signal power, where a fixed portion of the information signal is turned into *distortion noise* due to quantization errors in analog-to-digital converter (ADC), inter-carrier interference induced by phase noise, leakage from the mirror sub-carrier under I/Q imbalance, non-linearities in power amplifiers, etc. To be aligned with the ‘‘batch-processing’’ nature of

AI/ML algorithms and wireless communications simulators [22], we reformulate the signaling expressions in matrix-based format. To do so, we define the batch (with size  $K$ ) of information-bearing samples as  $\mathbf{s} \triangleq [s_1, s_2, \dots, s_K]^T$  corresponding to the batch of ground-truth information samples  $\mathbf{x}_0 \triangleq [x_0^{(1)}, x_0^{(2)}, \dots, x_0^{(K)}]^T$  with the underlying distribution  $\mathbf{x}_0 \sim q(\mathbf{x}_0)$ . Hence, the batch of received signals at the receiver can be expressed as

$$\mathbf{y} = \sqrt{P} \mathbf{H} \mathbf{s} + \boldsymbol{\zeta}, \quad (16)$$

where  $\mathbf{H} = \text{diag}(\mathbf{h})$ ,  $\mathbf{h} \triangleq [h^{(1)}, h^{(2)}, \dots, h^{(K)}]^T$  stands for the channel realizations vector corresponding to the transmission of information samples, and  $\boldsymbol{\zeta} \triangleq \mathbf{H} \boldsymbol{\tau}^t + \boldsymbol{\tau}^r + \mathbf{n}$  represents the effective noise-plus-distortion at the receiver with the conditional distribution  $\boldsymbol{\zeta} | \mathbf{h} \sim \mathcal{CN}(\mathbf{0}_K, \boldsymbol{\Sigma})$  and the covariance matrix  $\boldsymbol{\Sigma}$  given by  $\boldsymbol{\Sigma} = P(\kappa^t + \kappa^r) \mathbf{G} + \sigma^2 \mathbf{I}_K$ . We also define

$$\boldsymbol{\tau}^t \triangleq [\tau_1^t, \tau_2^t, \dots, \tau_K^t]^T \sim \mathcal{CN}(\mathbf{0}_K, \kappa^t \mathbf{P} \mathbf{I}_K), \quad (17)$$

$$\boldsymbol{\tau}^r \triangleq [\tau_1^r, \tau_2^r, \dots, \tau_K^r]^T \sim \mathcal{CN}(\mathbf{0}_K, \kappa^r \mathbf{P} \mathbf{G}), \quad (18)$$

which is conditionally Gaussian given the channel realizations  $\{h_k\}_{k \in [K]}$ , with  $\mathbf{G} = \text{diag}([|h_1|^2, |h_2|^2, \dots, |h_K|^2]^T)$ . Due to the fact that neural networks can only process real-valued inputs, we map complex-valued symbols to real-valued tensors, and rewrite (16) by stacking the real and imaginary components. This results in the following expression.

$$\tilde{\mathbf{y}} = \tilde{\mathbf{H}} \tilde{\mathbf{s}} + \boldsymbol{\nu}, \quad (19)$$

where

$$\tilde{\mathbf{y}} = \begin{bmatrix} \Re\{\mathbf{y}\} \\ \Im\{\mathbf{y}\} \end{bmatrix} \in \mathbb{R}^{2K}, \quad (20)$$

$$\tilde{\mathbf{s}} = \sqrt{p} \begin{bmatrix} \Re\{\mathbf{s}\} \\ \Im\{\mathbf{s}\} \end{bmatrix} \in \mathbb{R}^{2K}, \quad (21)$$

$$\tilde{\mathbf{H}} = \begin{bmatrix} \Re\{\mathbf{H}\} & -\Im\{\mathbf{H}\} \\ \Im\{\mathbf{H}\} & \Re\{\mathbf{H}\} \end{bmatrix} \in \mathbb{R}^{2K \times 2K}, \quad (22)$$

$$\boldsymbol{\nu} = \begin{bmatrix} \Re\{\boldsymbol{\zeta}\} \\ \Im\{\boldsymbol{\zeta}\} \end{bmatrix} \in \mathbb{R}^{2K}. \quad (23)$$

The receiver tries to obtain the information signals, using a decoding functionality  $f(\cdot)$ , which reverts the mapping carried out at the transmitter, either via conventional digital communication-based methods, or the DNN-based algorithms as in [18]. Accordingly, a noisy version of the ground-truth batch, denoted by  $\hat{\mathbf{x}}$  would be obtained as

$$\hat{\mathbf{x}} = f(\eta(g(\mathbf{x}))) \approx \mathbf{x}_0 + \mathbf{z}, \quad (24)$$

where  $\mathbf{z}$  denotes the unknown reconstruction error.

*Remark 1:* Notably, in extreme conditions due to low SNR regimes or highly mismatched transceiver and receiver due to large impairment levels, (where even error correction capabilities might not be satisfactory), the idea is to leverage the “denoising-and-generation” characteristics of DDPMs to help facilitate obtaining the ground-truth information signals.

*Remark 2:* The vanilla format of denoising process of DDPMs, as introduced in Section II, assumes starting the

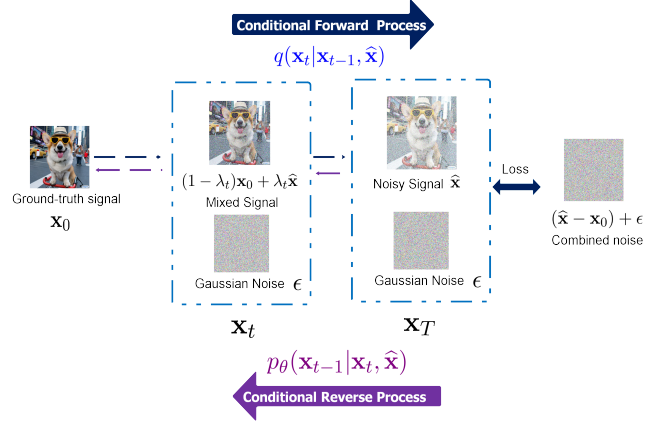


Fig. 3: Schematic of the Conditional DDPM Framework.

denoising-and-generation process with an isotropic Gaussian noise. However, in a practical wireless system, the reconstructed signals at the receiver are a degraded version,  $\hat{\mathbf{x}}$ , of the ground-truth information signals, not necessarily a pure isotropic Gaussian noise. This degradation is different in different distortion conditions such as different SNRs and impairment levels.

To address the above-mentioned challenges, we incorporate the noisy degraded signals into the denoising framework of the diffusion model, realizing a conditional DDPM. Accordingly, the denoising process is modified and the corresponding conditional diffusion and reverse processes are derived.

### B. Proposed Solution: CDiff for Enhanced Data Reconstruction

1) *Conditional Forward Process:* The idea of the employed conditional DDPM is to first incorporate the noisy degraded samples into the forward diffusion framework, so that we can learn, in the reverse diffusion, to remove the exact noise from  $\hat{\mathbf{x}}$  and refine the ground-truth information signals. For this, a weighted sum of the clean version of ground-truth samples  $\mathbf{x}_0$  and the noisy samples  $\hat{\mathbf{x}}$  are considered, using an interpolation hyperparameter  $\lambda_t$ , as shown in Fig. 3. Then the Markov chain-like transition model  $q(\mathbf{x}_t | \mathbf{x}_{t-1})$  in (1) is modified into a conditional forward diffusion process as follows.

$$q_{\text{cond}}(\mathbf{x}_t | \mathbf{x}_0, \hat{\mathbf{x}}) \sim \mathcal{N}\left(\mathbf{x}_t; (1 - \lambda_t) \sqrt{\alpha_t} \mathbf{x}_0 + \lambda_t \sqrt{\alpha_t} \hat{\mathbf{x}}, \delta_t \mathbf{I}\right), \quad (25)$$

Invoking (25), one can observe that this is a generalization of the vanilla forward diffusion process in (5), as we assume that the mean vector reflects an interpolation between the clean information signals  $\mathbf{x}_0$  and their noisy degraded version  $\hat{\mathbf{x}}$ . Accordingly,  $\lambda_t$  is set to start from 0 and gradually increased to  $\lambda_T \approx 1$ . Intuitively, this guides the diffusion model to pay more attention to learning the denoising process from noisy samples over time. According to (25), one can marginalize the conditional distributions over  $\hat{\mathbf{x}}$  and write

$$q_{\text{cond}}(\mathbf{x}_t | \mathbf{x}_0) = \int q_{\text{cond}}(\mathbf{x}_t | \mathbf{x}_0, \hat{\mathbf{x}}) p_{\hat{\mathbf{x}}}(\hat{\mathbf{x}} | \mathbf{x}_0) d\hat{\mathbf{x}}. \quad (26)$$



---

**Algorithm 1** Training algorithm
 

---

**Hyper-parameters:** Number of diffusion steps  $T$ , neural architecture  $\epsilon_\theta(\cdot, \cdot, t)$ , variance schedule  $\beta_t$  and  $\bar{\alpha}_t$ , and conditioning weights  $\lambda_t, \forall t \in [T]$ .

**Input:** Training samples: The pair of ground-truth information signal and its noisy decoded version from a dataset  $\mathcal{D}$ :  $(\mathbf{x}_0, \hat{\mathbf{x}}) \in \mathcal{D}$

**Output:** Trained model  $\epsilon_\theta(\cdot, \cdot, t)$ .

- 1: **while** the stopping criteria are not met **do**
  - 2: Randomly sample  $(\mathbf{x}_0, \hat{\mathbf{x}})$  from  $\mathcal{D}$
  - 3: Randomly sample  $t \sim \text{Unif}[T]$
  - 4: Randomly sample  $\epsilon \sim \mathcal{N}(\mathbf{0}, \mathbf{I})$
  - 5: Set  $\mathbf{x}_t = (1 - \lambda_t)\sqrt{\bar{\alpha}_t}\mathbf{x}_0 + \lambda_t\sqrt{\bar{\alpha}_t}\hat{\mathbf{x}} + \delta_t\epsilon$
  - 6: Take gradient descent step on
  - 7:  $\nabla_\theta \left\| \frac{1}{\sqrt{1-\bar{\alpha}_t}}(\lambda_t\sqrt{\bar{\alpha}_t}(\hat{\mathbf{x}} - \mathbf{x}_0) + \sqrt{\delta_t}\epsilon) - \epsilon_\theta(\mathbf{x}_t, \hat{\mathbf{x}}, t) \right\|^2$
  - 8: **end while**
- 

In order for the conditional diffusion  $q_{\text{cond}}(\mathbf{x}_t|\mathbf{x}_0)$  to become a generalization of the vanilla diffusion process  $q(\mathbf{x}_t|\mathbf{x}_0)$  in (5), one needs to set

$$\delta_t := (1 - \bar{\alpha}_t) - \lambda_t^2 \bar{\alpha}_t. \quad (27)$$

2) *Conditional Reverse Process:* The reverse process starts from  $\mathbf{x}_T$  as the degraded information signal  $\hat{\mathbf{x}}$  according to (25) while setting  $\lambda_T = 1$ , where we have  $p_{\text{cond}}(\mathbf{x}_T|\hat{\mathbf{x}}) \sim \mathcal{N}(\mathbf{x}_T, \sqrt{\bar{\alpha}_T}\hat{\mathbf{x}}, \delta_T\mathbf{I})$ . Considering a similar approach to (6), the conditional reverse process is considered to predict  $\mathbf{x}_{t-1}$  based on  $\mathbf{x}_t$  and  $\hat{\mathbf{x}}$ . This results in the following conditional reverse transition probability distribution.

$$p_{\text{cond}}(\mathbf{x}_{t-1}|\mathbf{x}_t, \hat{\mathbf{x}}) \sim \mathcal{N}(\mathbf{x}_{t-1}; \boldsymbol{\mu}_\theta(\mathbf{x}_t, \hat{\mathbf{x}}, t), \delta_t\mathbf{I}), \quad (28)$$

with  $\boldsymbol{\mu}_\theta(\mathbf{x}_t, \hat{\mathbf{x}}, t)$  formulating the estimated mean of the conditional reverse process. The expression for the conditional mean of the reverse process in (28) should be a generalization to the vanilla format, by incorporating the noisy signals  $\hat{\mathbf{x}}$  into the formulation as well. Therefore, with a similar expression to (12), the mean vector for each step of the conditional denoising can be expressed as a weighted sum of the denoised signal at step  $t$ ,  $\mathbf{x}_t$ , the conditional information regarding the degraded ground-truth,  $\hat{\mathbf{x}}$ , and the estimated noise  $\epsilon_\theta(\cdot, t)$ . Hence, we have

$$\boldsymbol{\mu}_\theta(\mathbf{x}_t, \hat{\mathbf{x}}, t) = \psi_x \mathbf{x}_t + \psi_{\hat{\mathbf{x}}} \hat{\mathbf{x}} - \psi_\epsilon \epsilon_\theta(\mathbf{x}_t, \hat{\mathbf{x}}, t), \quad (29)$$

It is shown in [23] that the values of coefficients  $\psi_x, \psi_{\hat{\mathbf{x}}}$ , and  $\psi_\epsilon$  can be estimated by solving the evidence lower bound (ELBO) optimization criterion, where we have

$$\psi_x = \frac{\delta_{t-1}(1 - \lambda_t)}{\delta_t(1 - \lambda_{t-1})} \sqrt{\bar{\alpha}_t} + (1 - \lambda_{t-1}) \frac{\delta_{t|t-1}}{\delta_t \sqrt{\bar{\alpha}_t}}, \quad (30)$$

$$\psi_{\hat{\mathbf{x}}} = (\lambda_{t-1} \delta_t - \frac{\lambda_t(1 - \lambda_t)}{1 - \lambda_{t-1}} \alpha_t \delta_{t-1}) \frac{\sqrt{\bar{\alpha}_{t-1}}}{\delta_t}, \quad (31)$$

$$\psi_\epsilon = (1 - \lambda_{t-1}) \frac{\delta_{t|t-1} \sqrt{1 - \bar{\alpha}_t}}{\delta_t \sqrt{\bar{\alpha}_t}}, \quad (32)$$

---

**Algorithm 2** Sampling algorithm
 

---

- 1: Sample  $\mathbf{x}_T \sim \mathcal{N}(\mathbf{x}_T; \sqrt{\bar{\alpha}_T}\hat{\mathbf{x}}, \delta_T\mathbf{I})$
  - 2: **for**  $t = T, \dots, 1$  **do**
  - 3:  $\mathbf{z} \sim \mathcal{N}(\mathbf{0}, \mathbf{I})$
  - 4:  $\mathbf{x}_{t-1} = \psi_x \mathbf{x}_t + \psi_{\hat{\mathbf{x}}} \hat{\mathbf{x}} - \psi_\epsilon \epsilon_\theta(\mathbf{x}_t, \hat{\mathbf{x}}, t) + \sqrt{\delta_t} \mathbf{z}$
  - 5: **end for**
  - 6: **return**  $\mathbf{x}_0$
- 

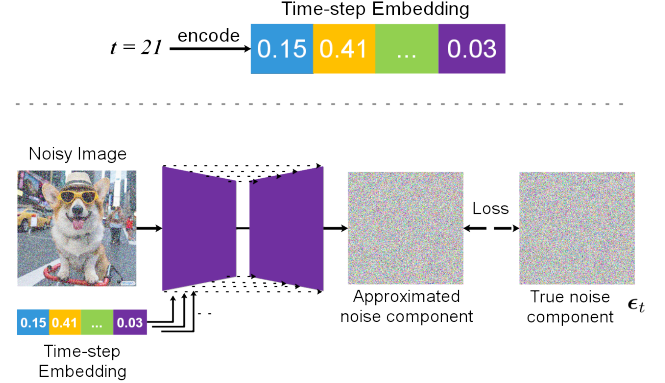


Fig. 4: General description of training the diffusion model and the notion of time embedding. Each time-step is mapped (via positional embedding) to an embedding vector, which is then incorporated into the hidden layers of the neural network. The figure shows time-step  $t = 21$  as an example.

where  $\delta_{t|t-1} \triangleq \delta_t - \left(\frac{1-\lambda_t}{1-\lambda_{t-1}}\right)^2 \alpha_t \delta_{t-1}$ . As such, the loss function for the conditional model is expressed as

$$\mathcal{L}_t^{\text{cond}} = \mathbb{E}_{\mathbf{x}_0, \epsilon, \hat{\mathbf{x}}} \left\| \left( \frac{\lambda_t \sqrt{\bar{\alpha}_t}}{\sqrt{1 - \bar{\alpha}_t}} (\hat{\mathbf{x}} - \mathbf{x}_0) + \frac{\sqrt{\delta_t}}{\sqrt{1 - \bar{\alpha}_t}} \epsilon \right) - \epsilon_\theta(\mathbf{x}_t, \hat{\mathbf{x}}, t) \right\|_2^2, \quad (33)$$

where  $\epsilon \sim \mathcal{N}(\mathbf{0}, \mathbf{I})$ . Intuitively speaking, the loss function in (33) is designed such that the conditional DDPM learns, over the denoising steps, to estimate both the Gaussian noise  $\epsilon$  and the residual errors of estimating  $\hat{\mathbf{x}}$ , i.e.,  $\hat{\mathbf{x}} - \mathbf{x}_0$ . Therefore, the coefficients for  $(\hat{\mathbf{x}} - \mathbf{x}_0)$  and  $\epsilon$  are chosen similar to the coefficient of  $\hat{\mathbf{x}}$  and the standard deviation of the diffusion process as in (25), respectively. According to (27)–(33), the training and sampling algorithms are summarized in Algorithm 1 and Algorithm 2, respectively. A visual description of the training phase is also exhibited in Fig. 4.

#### IV. NUMERICAL RESULTS

In this section, we provide different numerical evaluations to highlight the performance of our proposed approach in different scenarios and compared to different baselines. We also evaluate the *robustness* of our proposed scheme under low-SNR regimes.

### A. Experimental Setup

1) **Communication Setup:** Our scheme is implemented in conjunction with the NVIDIA Sionna simulator [22] to show the compatibility of the scheme with a practical communication system. To elaborate, after that the diffusion model is trained offline using Algorithm 1, it is plugged into the end of the receiver block of the Sionna simulator as shown in Fig. 1. In the evaluations, both scenarios of DNN-based receiver, known as Sionna’s neural receiver, and also the conventional receiver are considered in the evaluations.<sup>4</sup> We consider 64-QAM modulation symbols with 5G low density parity check coding (LDPC) [22] for the modulation and coding of the transmission scheme. The transmit SNR is defined as

$$\Gamma = 10 \log_{10} \left( \frac{P}{\sigma^2} \right) \text{ dB}. \quad (34)$$

Without loss of generality, we normalize the transmit power by setting the average signal power to  $P = 1$  for all experiments, while varying the SNR by setting the standard deviation (std) of noise  $\sigma$  [24]. Following the experimentally-validated model of [21], we consider the impairment levels in the range  $[0, 0.15^2]$  [1], [4], where smaller values correspond to less-impaired transceiver hardware.

2) **Learning Setup:** Evaluations are carried out on MNIST dataset<sup>5</sup> (resized to  $32 \times 32$ ). The dataset is split into 60,000 training images and 10,000 testing images of hand-written digits [25]. The corresponding dataset  $\mathcal{D}$  in Algorithm 1, is then obtained by transmitting the training samples of MNIST over the Sionna’s simulator and obtain the decoded signals at the receiver’s output, and then pairing each of the ground-truth samples with their degraded version to create  $(\mathbf{x}_0, \hat{\mathbf{x}}) \in \mathcal{D}$ . For validation of our numerical analysis, mean-squared error (MSE) and PSNR metrics are studied in this paper. These metrics measure the quality of reconstruction, where a higher(lower) PSNR(MSE) indicates better quality.

Training of our scheme can be carried out via two different training strategies, i.e., varying training SNR (simulating the system with different transmit SNRs), or fixed training SNR (fixing the communication scenario to a determined SNR). Our validations in terms of the PSNR metric showed that the performance of the fixed training SNR scenario saturates too early during the validation phase. Therefore, we choose the varying scenario, where we set  $-15 \leq \Gamma^{\text{train}} \leq 15$  dB by trial and error over different ranges of SNRs. Notably, having training samples  $(\mathbf{x}_0, \hat{\mathbf{x}})$  from a wide range of communication SNRs and the typical range of transmitter and receiver impairment levels  $\kappa^{t,r} \in [0, 0.15^2]$  (See Table I) indicates that the wireless conditions are implicitly taken into account as the conditioning of our model. This way, we incorporate the conditions of a practical wireless system into account.

For the choice of neural network for our CDiff model, we follow the model employed in [9], and adopt the U-Net

TABLE I: Parameters of the communication setup.

Parameter	Value
Simulation Setup	NVIDIA Sionna Link-level Simulator [22]
Modulation scheme	64 QAM [22]
Coding scheme	5G LDPC [22]
Training SNR	$[-15, 15]$ dB
Impairment level	$[0, 0.15^2]$ [1], [4], [21]

architecture [26] as our denoising neural network  $\epsilon_\theta(\mathbf{x}_t, \hat{\mathbf{x}}, t)$  with input size 32 and depth of 4. The employed neural network is supposed to take the distorted image at each time step, and output the predicted noise with the same size as the input image. The U-Net architecture matches well with this requirement. It consists of a contracting path and an expansive path, which respectively capture contextual information and reduce the spatial resolution of the input, and then up-samples the feature maps, while also performing convolutional operations [26]. Additionally, it introduced residual connections between the encoder and decoder, which greatly improves the gradient flow. The training is carried out for 10 epochs over  $T = 200$  steps, and using adaptive moment estimation (Adam) optimizer with learning rate  $\lambda = 10^{-3}$ . To stabilize the training process, exponential moving average (EMA) method is implemented [27] for model update during training. This helps maintain a form of “model momentum.” Specifically, instead of directly updating model’s weights, a copy of the previous weights is kept, and the weighted average between the previous and new version of the weights are calculated for the model update. For the conditioning weights  $0 < \lambda_t < 1$ , we consider a linear scheduling over  $T = 200$  steps. For the variance scheduling  $\beta_t$ , we also consider a linear scheduling, starting from  $\beta_0 = 0.0001$  to  $\beta_T = 0.0095$ . We note that the values for the variance scheduling were obtained based on trial-and-error over different scheduling formats. To the best of our knowledge, there does not exist a unified generic solution for the choices of variance scheduling in the diffusion model literature, and it depends on the specific problem to which the diffusion model is applied. To enable employing only one neural network for the entire denoising steps, instead of training  $T$  distinct models for each time-step  $t \in [T]$ , we share the parameters of the neural network across time-steps. More specifically, as shown in Fig. 4, we encode the time-steps  $t \in [T]$  and input it to each hidden layer of our neural network as a positional embedding [9]. The output of the hidden layers are then multiplied by the time embeddings [9], [11], [14]. Intuitively, this makes the model “know” at which particular time-step it is operating for every sample in the batch. To summarize, Tables I and II highlight the experimental setup and hyper-parameters and metrics used for the simulation.

### B. Baseline methods used for comparison

The following baselines are employed for comparison with our proposed approach.

<sup>4</sup>One interesting direction would be to propose a framework in which the forward and reverse process of diffusion training are directly incorporated into the communication simulator. This requires modeling the conditional probability distribution of data transmission and reconstruction as modified forward and reverse diffusion processes, respectively, which will be studied in our future works.

<sup>5</sup><http://yann.lecun.com/exdb/mnist>

TABLE II: Hyper-parameters of the learning setup.

Parameter	Value
Dataset	MNIST [25]
Train-test split	60000 - 10000
Neural architecture	U-Net with depth 4 (32, 64, 128, 256) [9], [26]
Total denoising steps	$T = 200$
Training epochs	10
variance scheduling	linear for $(\beta_0, \beta_T) = (0.001, 0.0095)$ [9]
Learning rate	0.001 with Adam optimizer [27]

- DNN-based receiver [18] incorporated into Sionna’s simulator<sup>6</sup>. This baseline is studied for both qualitative and quantitative comparisons in Figs. 6 and 8, respectively. For the DNN-based receiver baseline, we are inspired by the network architecture proposed in [18], and since we have employed our diffusion model at the receiver, we only exploit the receiver DNN of [18] and fine-tune it for benchmarking, so that we can have a fair comparison. Three hidden linear layers with 64 neurons and rectified linear unit (ReLU) activation functions are implemented, trained for 5000 iterations with learning rate 0.01. Based on our trial and errors, increasing the depth of the conventional DNN, or the number of hidden neurons does not result in any significant improvement in its performance. We show that our proposed model outperforms this baseline since the CDiff exploits the generative prior knowledge regarding the underlying distribution of the ground-truth information signals. However, the DNN receiver does not take the “content”, nor any prior knowledge of the information signals into account when decoding the information bits.
- VAE-based reconstruction. VAEs as another state-of-the-art GenAI-based decoding approach, which are famous for image reconstruction, are compared with our DDPM approach. This is quantitatively studied in Fig. 7. As mentioned earlier, our approach considers the “contents” of the transmitted signal during denoising and reconstruction. Therefore, to have a fair comparison from the perspective of “prior knowledge” utilization, we consider this baseline, which also considers the prior knowledge about the underlying distribution of the ground-truth when reconstructing. The VAE’s loss function is composed of two parts, i.e., the reconstruction loss and the Kullback-Leibler (KL) divergence loss. The former measures the difference between the original data and the reconstructed output generated by the decoder, while the latter measures the difference between the learned probability distribution and the predefined prior distribution. For the “contracting path,” four 2D convolutional layers (Conv2D) are implemented with 32, 64, 64, and 64 filters, respectively, with kernel size of  $3 \times 3$ , and ReLU activation functions, followed by a flattening layer and a dense layer of size 32 (to combine the down-sampled learned features before entering the latent space). Two dense layers further generate the parameters of the Gaussian distribution in the latent space (a.k.a. the mean vector  $\mu$  and log variance vector  $\sigma$  which

represent the compressed latent features of the input), with latent space dimension  $\text{Dim}$  set to 5 and 20 for different scenarios (see Fig. 7). The decoder reconstructs the images from the latent representation, by exactly mirroring the encoder in reverse, by progressively up-scaling the compressed data back to its original dimension. Accordingly, the architecture is implemented by a dense layer and a reshape layer to up-scale to a higher dimension, and then followed by de-convolutional layers (Conv2DTranspose), to further upscale and refine the data to reconstruct the original input. We show the superior performance of our approach compared this baseline, thanks to the high-quality sampling characteristic of diffusion models.

- Conventional Receiver (Naive scheme). This baseline is studied for qualitative comparison (data visualization in Fig. 5), as well as quantitative comparisons (Figs. 9 and 10). Our proposed scheme complements this baseline in a way that instead of employing error correction codes with low code rates to improve data decoding in extreme channel conditions, our proposed scheme can be employed while preserving the data rate. We show that we can maintain higher data rates while also improving the reconstruction quality. We also show that the functionality of the proposed CDiff can be exploited to compensate for the underlying errors within the noisy data at the receiver, outperforming the channel codes in conventional receivers.

In what follows, we show how our proposed method outperforms or complements the existing approaches.

### C. Qualitative Comparisons: Data Visualization

Fig. 5 visualizes the performance of our conditional DDPM-aided reconstruction enhancement scheme. For this figure, we consider the extreme condition of  $\Gamma = 0$  dB channel SNR, with the transmitter’s impairment level  $\kappa^t = 0.1$  and the receiver’s impairment level of  $\kappa^r = 0.15$ . As can be seen from the figure, under such extreme conditions, the naive format of a communication system cannot perform well in removing the noise and distortions to obtain a clean denoised version of the ground-truth information signals (Fig. 5-(b)). In such scenarios, our proposed diffusion-aided scheme can improve the reconstruction of images by removing the noise and distortions conditioned on the degraded signals. This results in a significant improvement in the decoding performance. This improvement is actually obtained via exploiting the prior knowledge learnt by our conditional DDPM. One might argue that in such cases, we can play with the coding rate and employ stronger error correction codes with lower code rates. However, this can significantly reduce the data rate, while stronger error correction codes might not necessarily work well under such extreme conditions either. In the subsequent figures, we numerically study this and we show that the DDPM outperforms those schemes in low SNR regimes.

Fig. 6 visualizes the output of our proposed diffusion-aided scheme, compared to a DNN-based receiver as benchmark [18]. For this experiment, we set  $\Gamma = 5$  dB SNR and the

<sup>6</sup>[https://nvlabs.github.io/sionna/examples/Sionna\\_tutorial\\_part2.html](https://nvlabs.github.io/sionna/examples/Sionna_tutorial_part2.html)



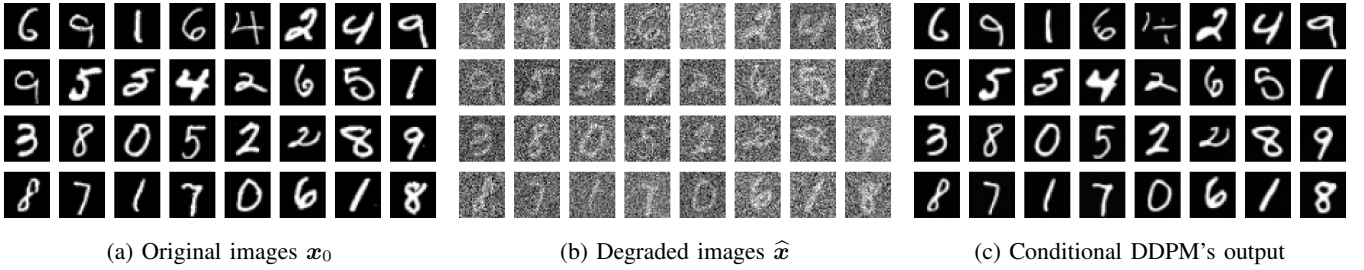


Fig. 5: Data visualization for the performance evaluation of the proposed scheme for image reconstruction enhancement. From left to right, the ground-truth information signals  $x_0$ , the degraded version  $\hat{x}$  of the signals decoded at the output of the Sienna’s simulator (before DDPM-based reconstruction), and the final reconstructed signals via our method are shown, respectively.

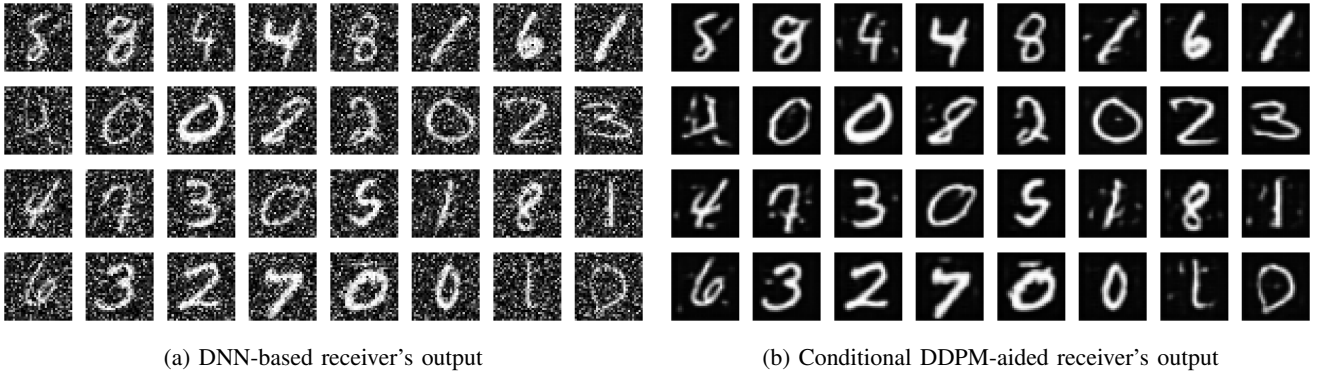


Fig. 6: Comparison between the DNN-based receiver [18] and our DDPM-aided model for image reconstruction.

transmitter’s impairment level  $\kappa^t = 0.1$  and the receiver’s impairment level of  $\kappa^r = 0.15$ . Notably, compared to the DNN benchmark our scheme highlights a considerably better performance in obtaining clean samples of the information signals, by removing noise and other residual decoding errors. This is due to the fact that the diffusion-based method exploits the generative prior knowledge about the underlying distribution of the ground-truth information signals. However, a DNN-based receiver as proposed in [18] does not take the “content”, nor any prior knowledge of the information signals into account when decoding the information bits. We further emphasize that numerical comparisons between our scheme and the DNN benchmark are provided in the subsequent figures.

#### D. Quantitative Comparisons: Reconstruction Performance

In this subsection, we numerically assess the reconstruction performance of the proposed scheme in different scenarios.

Fig. 7 shows the reconstruction performance in terms of PSNR metric for our proposed conditional DDPM-based approach, compared to the VAE-based reconstruction baseline which was introduced in Section IV-B. For case I to III, we consider  $(\kappa^t, \kappa^r) = (0.01, 0.01)$ ,  $(\kappa^t, \kappa^r) = (0.05, 0.1)$ , and  $(\kappa^t, \kappa^r) = (0.05, 0.15)$ , respectively. In the figure, VAE-Dim shows the latent space dimension of the implemented VAE, where higher latent dimensions can offer a slightly better reconstruction quality. As can be seen from the figure, our proposed DDPM outperforms the VAE baseline with more than 40% improvement in PSNR metric. This is due to

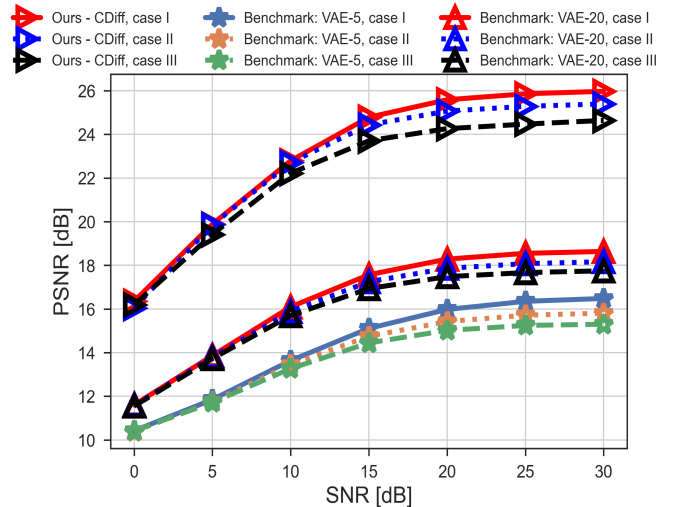


Fig. 7: Reconstruction performance in terms of PSNR for DDPM vs. VAE.

the high-quality sampling characteristic of diffusion models, while VAEs lack this important generative feature [28]. To elaborate, in contrast to VAEs, diffusion models maintain high sample quality and strong mode coverage, because of their unique feature for *fine-grained denoising* which is realized via the reverse diffusion process. This makes them suitable for the applications that interact with end-users and require high quality data reconstruction and generation. We further note that the saturation observed in the PSNR trends over SNR

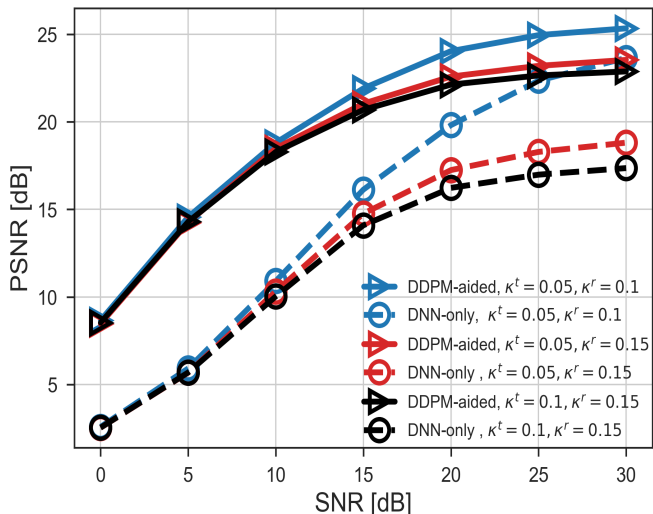


Fig. 8: Reconstruction performance in terms of PSNR: Comparison between generative (DDPM-based) learning approach vs. discriminative (DNN-based) learning approach.

is due to the so-called “ceiling phenomena” in the literature of hardware-impaired communications [21]. To elaborate, by increasing the SNR, the effect of channel noise becomes negligible compared to the effect of residual impairments within the RF chain of communication systems, hence the performance metrics become saturated [21]. As can be seen from the figure, the PSNR increases with the increase in SNR, due to having less noise communication, which makes it easier for the employed diffusion to denoise and reconstruct when facing with a less degraded signal. In addition, lower impairment levels indicate higher qualities for the transceiver hardware which results in less mismatches between the transmitted signals and the decoded ones, thus improving the reconstruction performance. Generally speaking, the proposed scheme shows a *near-invariant* performance with respect to the hardware impairments (as we can see the slight change in PSNR with respect to the three scenarios). This is further studied in Fig. 11.

Fig. 8 evaluates the reconstruction performance of our proposed approach when it is employed in conjunction with the Sionna’s neural receiver<sup>7</sup>, compared to the non-DDPM approach which simply employs the Sionna’s neural receiver without any diffusion enhancement. The figure highlights about 10 dB improvement in low-SNR regimes, as well as more than 5 dB improvement in higher SNRs, when using our generative model. This is due to the fact that our DDPM-based scheme takes into account the entire underlying distribution of the ground-truth signals that are supposed to be sent over the wireless channel. However, the conventional DNNs neglect the underlying “content” of the information signals, and simply care about the “bit-wise” transmission, using discriminative loss functions, such as binary cross-entropy, rather than a content-wise” approach.

Fig. 9 demonstrates the image reconstruction error, in terms

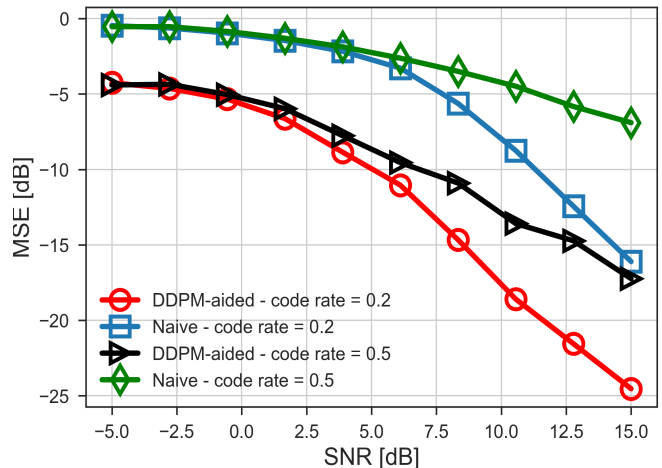


Fig. 9: Reconstruction performance in terms of MSE between the original images and the reconstructed ones.

of the mean squared error (MSE) versus SNR for  $\kappa^t = \kappa^r = 0.25$ . The figure shows that under extreme conditions (low-SNR and mid-SNR regimes and highly-impaired communications), a naive scheme (without our proposed diffusion model) cannot perform well in terms of the image reconstruction, even if the error correction rate is decreased from 0.5 to 0.2. When the conditional DDPM is employed, the reconstruction is enhanced significantly, by more than 10 dB. This is due to the fact that our scheme leverages the denoising capabilities of diffusion models, as well as being conditioned on the degraded output of a naive communication system, which guides the diffusion to improve the data decoding and reconstruction as shown in the figure. The figure suggests that instead of employing error correction codes with lower code rates, to improve the data decoding quality, our proposed scheme can be employed while preserving the data rate. As can be seen from the figure, more than 5 dB performance improvement, as well as 2.5 times higher data rates can be achieved under low SNR regimes with our proposed scheme, instead of reducing the code rate from 0.5 to 0.2 in a naive scheme. This is applicable to scenarios in which data rates and reliable communications are assumed to be taken into account at the same time. Also note that although the gap between a naive scheme with lower code rate (blue curve) and the DDPM-aided scheme with code rate of 0.5 (black curve) decreases as the SNR increases, the figure shows that if we employ the DDPM, the same performance can be achieved, while we do not even need to decrease the data rate.

Fig. 10 shows the reconstruction performance between the original images and the reconstructed ones for two different impairment levels. In this experiment, we aim to show that the functionality of the proposed CDiff can be exploited to compensate for the underlying errors within the noisy reconstructed images obtained at the receiver, instead of employing channel codes. As can be seen from the figure, by employing our conditional DDPM, the quality of the information signals (images in our scenario) can be improved more than the case where error correction codes are employed. For instance, by

<sup>7</sup>[https://nvlabs.github.io/sionna/examples/Sionna\\_tutorial\\_part4.html](https://nvlabs.github.io/sionna/examples/Sionna_tutorial_part4.html)

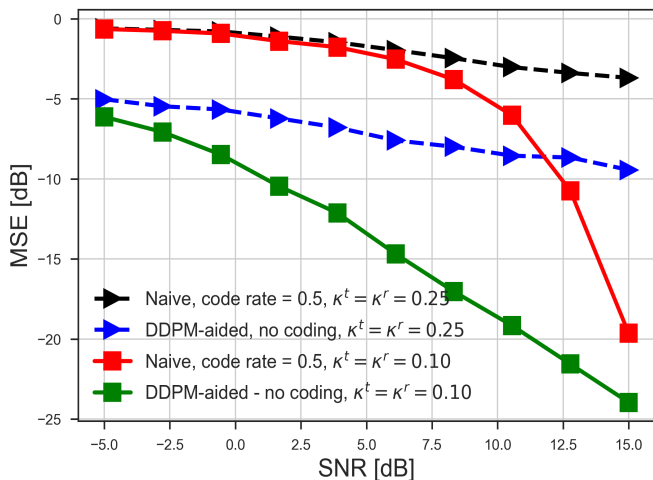


Fig. 10: Reconstruction performance between the original images and the reconstructed ones for different impairment levels: Diffusion models vs. channel codes.

employing our proposed scheme, more than 10 dB improvement in reconstruction performance can be achieved at 5 dB SNR and impairment level 0.1. This can be explained due to the fact that channel codes do not take into account the underlying structure and the contents of the information signals that are transmitted over the channel. However, our proposed scheme essentially considers the content of the transmitted signals when carrying out the denoising and reconstruction. Also note that error correction codes require sending redundancy bits which decrease the data rate, while our diffusion-based scheme has achieved better performance without the need for transmitting such redundancy bits. Therefore, the figure indicates that our scheme can improve the reliability of the communication systems, while saving the resources for only transmitting information bits. Obviously, this performance improvement comes with a trade-off in the sense that the DDPM model requires higher computation resources than the error correction codes. Nevertheless, one should note that the *computations related to error correction codes are implemented in both of the communication sides, i.e., the transmitter (the encoder part), and the receiver (the decoder part), while the proposed diffusion is only employed and run at the receiver side.*

*Remark 3: We remark that the outperformance of our scheme compared to the traditional channel codes comes with a trade-off. DDPMs may fall short in sampling speed due to the stepwise denoising process. Although this appears to limit the wide adoption of diffusion models for some applications, there already exists an active line of research focusing on accelerating the generation process. Such computation-efficient variants of diffusion framework, such as [4], can help facilitate the applicability of diffusion models to a wide range of real-world wireless scenarios.*

### E. Complexity Analysis

We further address the potential computational overhead of implementing DDPMs to highlight the complexity-performance trade-off compared with the traditional error correction coding methods.

1) *Traditional channel codes:* According to the coding theory, the encoding of LDPC codes is typically performed using a generator matrix  $\mathbf{G}$  that transforms the input information bits into codewords via multiplying the input stream by the 5G LDPC matrices. The complexity of encoding an LDPC code is proportional to the number of non-zero entries in the generator matrix, and is approximated by  $\mathcal{O}(n)$ , where  $n$  is the length of the codeword. The complexity of LDPC decoding is more computation-intensive than encoding, because of the *iterative* algorithms of decoding. According to coding theory [29], the complexity of LDPC decoding depends on the number of non-zero entries in the parity-check matrix  $\mathbf{H}$ , which represents the edges in the bipartite graph used for message passing in the belief propagation (BP) algorithm [29], [30]. The BP algorithm iteratively updates the likelihoods (beliefs) for each bit, passing messages between the variable nodes (representing bits) and check nodes (representing parity checks) in a bipartite graph. Then the complexity per iteration is proportional to the number of edges,  $E$ , in the graph. For an LDPC with the length of the codeword denoted by  $n$ , the complexity per iteration is approximately  $\mathcal{O}(E)$ , and since the number of edges  $E$  is typically proportional to  $n$  (due to the sparsity of  $\mathbf{H}$ ), the computation complexity is  $\mathcal{O}(n \cdot I)$ , where the number of iterations  $I$  for LDPC decoding typically depends on the target error-correction performance. Assuming  $F$  floating-point operations (FLOPs) per message update on an edge (for calculating likelihoods and probabilities), the total FLOPs for the traditional error correction would be

$$\text{FLOPs}^{\text{LDPC}} = \mathcal{O}(I \cdot n \cdot F). \quad (35)$$

2) *DDPM's complexity:* The computational complexity of a U-Net can generally be analyzed in terms of the number of FLOPs for its convolutional layers within the contractive and expansive paths [26], [31]. Key parameters that influence the complexity are input size (considering the spatial dimensions of the input image as  $H \times W$  for height and width), and depth of the U-Net architecture,  $D$ . This reflects the number of down-sampling and up-sampling stages in the U-Net. For a U-Net with depth  $D$ , the input size is halved at each down-sampling layer in the contracting path, and the number of channels doubles [26]. Hence, assuming  $k \times k$  filter size and  $C$  as the number of input channels, the FLOPs at each layer  $i \in [D]$  of the contractive (down-sampling) path can be calculated as

$$\text{FLOPs}_i^{\text{UNet,ds}} = k^2 \left( \frac{H}{2^i} \cdot \frac{W}{2^i} \right) \cdot (2^{i-1}C) \cdot (2^iC). \quad (36)$$

The reverse happens in the up-sampling (expansive path), and hence we have

$$\text{FLOPs}_i^{\text{UNet,us}} = k^2 \left( \frac{H}{2^{D-i}} \cdot \frac{W}{2^{D-i}} \right) \cdot (2^{D-i}C) \cdot (2^{D-i-1}C). \quad (37)$$

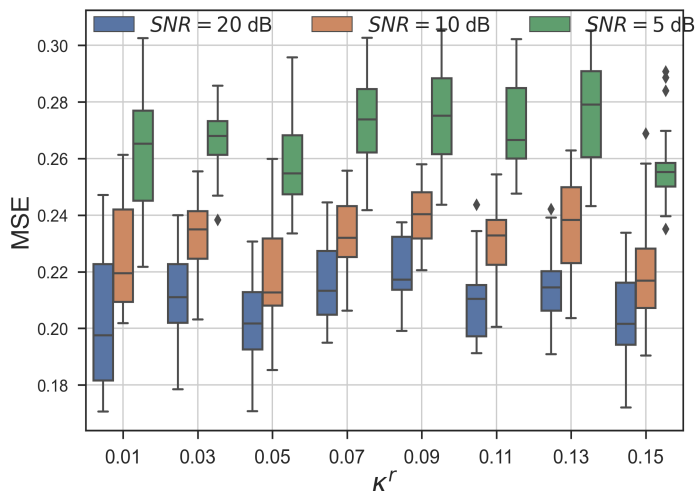


Fig. 11: MSE between the original images and the reconstructed ones for different levels of hardware impairment.

In addition to up/down-sampling, U-Net architecture also maintains the skip connections, the complexity of which is negligible with respect to that of the convolution layers. Hence, summing over all the down-sampling and up-sampling layers for a depth  $D$  U-Net, the total complexity of the U-Net architecture can be approximated by [31]

$$\text{FLOPs}^{\text{U-Net}} \approx \mathcal{O}(H \cdot W \cdot C^2 \cdot D). \quad (38)$$

Recall that in the denoising and reconstruction process of our proposed CDiff method, the U-Net is applied at each of the  $T$  diffusion steps to gradually denoise the data. At each step, the complexity is that of running the U-Net once. Therefore, the total complexity of the diffusion model is the complexity of the U-Net multiplied by the number of diffusion steps

$$\text{FLOPs}^{\text{DDPM}} \approx \mathcal{O}(T \cdot H \cdot W \cdot C^2 \cdot D). \quad (39)$$

This indicates that the complexity grows linearly with the depth  $D$  of the network, and linearly with the spatial size of the input  $H \times W \times C^2$ .

3) *Comparison*: If we assume the number of denoising steps  $T$  to be equivalent/counterpart to the number of decoding iterations,  $I$ , in traditional decoding, and the input spatial dimensions  $H \times W \times C^2$  in the DDPM method as the equivalent counterpart to the size of the input data-stream to the LDPC error correction decoding (input codeword length), the computation complexity of the DDPM-based approach depends on how deep the neural architecture of the diffusion framework is. This is reflected as the depth  $D$  of the network in (39). This shows that, similar to any other AI/ML models applied to wireless problems, the complexity overhead of diffusion-based models is also dominated by nothing except the underlying neural network architecture. This also highlights the importance of studying efficient implementations of diffusion architectures and quantization and pruning techniques for the wide adoption of such models in real-world wireless problems.

Finally, Fig. 11 studies the effect of different impairment levels on the reconstruction performance of our scheme over

Rayleigh fading channels. For this figure, we set  $\kappa^t = 0.05$  and vary the impairment level of the receiver,  $\kappa^r$ , over the typical ranges specified in Ref. [21]. The reconstruction results are obtained in terms of MSE metric over 20 realizations of the system. The figure highlights an important characteristic of our proposed scheme. Our DDPM-based communication system is *robust* against hardware distortions, since the reconstruction performance does not change with the increase in the impairment level. Notably, our scheme showcases a *near-invariant* reconstruction performance with respect to noise and impairment levels. This is achieved due to the so-called “variance scheduling” of diffusion framework in (3), which allows the system to become robust against a wide range of distortions caused by channel and hardware impairments.

#### F. Further analysis and discussions on model’s robustness

We would like to provide some further discussions and highlight how the proposed CDiff method offers a robust performance under varying conditions, demonstrating its reliability in practical scenarios. The fact that the model adapts to varying noise conditions and is effective in low-SNR regimes can be addressed by the compilation of the following reasons.

- DDPMs maintain the **variance scheduling** in the forward diffusion mechanism, wherein the samples are diffused at each time-step  $t \in [T]$  according to  $q(\mathbf{x}_t|\mathbf{x}_{t-1})$  in (1). Invoking (3)–(6), one can model the forward diffusion according to a “diffusion SNR”  $\gamma^{\text{DDPM}}(t) = \frac{1-\bar{\alpha}_t}{\bar{\alpha}_t}$ . The mathematical relations between the diffusion SNR, and the communication SNR would be an interesting direction to study in the future. However, the important point here is that in practice, the receiver of a communication system might not have any prior knowledge regarding the levels of RF impairments and communication SNRs. The forward diffusion does not consider any form of pre-defined hardware impairment levels or communication SNRs either. This is exactly the point of forward diffusion in our scheme. We purposefully “diffuse” Gaussian noise which maintains the maximum entropy, thus maximum uncertainty from the information-theoretic perspective, and then the DDPM tries to make itself “robust” against a wide range of uncertainties. This intuitively reflects a robust performance over a wide range of scenarios as shown in the paper.
- The concept of **conditioning** in our scheme offers an additional level of robustness for the system. We incorporated the noisy decoded data  $\hat{\mathbf{x}}$  into the diffusion framework to learn to remove the exact noise from  $\hat{\mathbf{x}}$  and recover the ground-truth  $\mathbf{x}$ . This way, the CDiff learns to estimate both the Gaussian noise  $\epsilon$  and the residual errors  $\hat{\mathbf{x}} - \mathbf{x}_0$ . Moreover, this further allowed us to consider different communication SNRs during the training as described in IV-A. Hence, this conditioning has helped us incorporate the conditions of a practical wireless system into account, making the system more robust to different conditions in the inference phase.



- The notion of **time embedding** in the DDPM also reinforces the model robustness. Considering the variance scheduling  $\beta_t$ , each time-instance has a unique mapping to a specific noise variance. Hence, intuitively speaking, each time-step equivalently corresponds to a specific level of noise-plus-distortion in the batch of received signals. Incorporating the time-steps  $t \in [T]$  into our neural network as explained in Section IV-A, makes the model “know” at which particular time-step is operating for each level of channel noise, making it robust against different SNR and/or impairment levels. This notion  $t$  is also reflected in the loss function of our model in (35), so data samples with different levels of “noisiness” are processed at different time-steps during training.

## V. CONCLUSIONS

In this paper, we have proposed conditional DDPMs to enhance the data reconstruction in wireless communication schemes. The key idea is to leverage the generative prior of diffusion models to learn a noisy-to-clean transformation of the information signal, conditioned on the degraded version of the receiver data. The proposed scheme is applicable to scenarios in which a prior knowledge of the information signals is available, e.g., in multimedia transmission. Our numerical results on MNIST dataset have shown that instead of employing complicated channel codes that reduce the information rate, CDiffs can be employed that improve reliable data transmission, especially under extreme channel conditions due to low SNR, or hardware-impaired communications. Our evaluations have been carried out using the NVIDIA Sionna simulator, where it has been shown that more than 10 dB improvement as well as 2 times higher data rates can be achieved under low SNR regimes with our proposed scheme, compared to a conventional error correction-based data transmission and reconstruction. Moreover, we highlight the outperformance of the proposed generative learning approach compared to the conventional contrastive learning models based on DNNs.

## REFERENCES

- [1] M. Letafati, S. Ali, M. Latva-aho, “Denoising diffusion probabilistic models for hardware-impaired communications,” *2024 IEEE Wireless Communications and Networking Conference (WCNC)*, Dubai, United Arab Emirates, 2024, pp. 1-6.
- [2] N. Van Huynh et al., “Generative AI for physical layer communications: A survey,” *IEEE Transactions on Cognitive Communications and Networking*, vol. 10, no. 3, pp. 706–728, June 2024.
- [3] M. Letafati, S. Ali, and M. Latva-aho, “Diffusion Models for Wireless Communications,” *arXiv preprint arXiv:2310.07312*, Dec. 2023.
- [4] M. Letafati, S. Ali, and M. Latva-Aho, “Diffusion model-aided data reconstruction in cell-free massive MIMO downlink: A computation-aware approach,” *IEEE Wireless Communications Letters*, vol. 13, no. 11, pp. 3162–3166, Nov. 2024.
- [5] M. Chafii, L. Bariah, S. Muhaidat, and M. Debbah, “Twelve scientific challenges for 6G: Rethinking the foundations of communications theory,” *IEEE Communications Surveys & Tutorials*, vol. 25, no. 2, pp. 868–904, Second quarter 2023.
- [6] M. Merluzzi et al., “The Hexa-X project vision on artificial intelligence and machine learning-driven communication and computation co-design for 6G,” *IEEE Access*, vol. 11, pp. 65620–65648, Jun. 2023.
- [7] 3GPP Release 18, “Study on Artificial Intelligence (AI)/Machine Learning (ML) for NR Air Interface RAN,” Meeting #112, Athens, Greece, Tech. Rep., 27th February – 3rd March 2023.
- [8] S. Ali, et al., “6G white paper on machine learning in wireless communication networks,” *arXiv preprint arXiv:2004.13875*, 2020.
- [9] J. Ho, A. Jain, and P. Abbeel, “Denoising diffusion probabilistic models,” *Advances in Neural Information Processing Systems*, vol. 33, pp. 6840–6851, 2020.
- [10] B. Levac, A. Jalal, K. Ramchandran, and J. I. Tamir, “MRI reconstruction with side information using diffusion models,” *arXiv:2303.14795*, Jun. 2023. [Online]. Available: <https://arxiv.org/abs/2303.14795>.
- [11] L. Yang, et al., “Diffusion models: A comprehensive survey of methods and applications,” *arXiv:2209.00796*, Mar. 2023. [Online]. Available: <https://arxiv.org/abs/2209.00796>.
- [12] Y. Liu, H. Du, D. Niyato, J. Kang, Z. Xiong, D. I. Kim, A. Jamalipour, “Deep generative model and its applications in efficient wireless network management: A tutorial and case study,” *IEEE Wireless Communications*, vol. 31, no. 4, pp. 199–207, Aug. 2024.
- [13] M. Kim, R. Fritschek, and R. F. Schaefer, “Learning end-to-end channel coding with diffusion models,” *26th International ITG Workshop on Smart Antennas and 13th Conference on Systems, Communications, and Coding (WSA & SCC 2023)*, Braunschweig, Germany, Feb. 27 – Mar. 3, 2023, pp. 1–6.
- [14] M. Arvinte and J. I. Tamir, “MIMO channel estimation using score-based generative models,” *IEEE Trans. Wireless Commun.*, vol. 22, no. 6, pp. 3698–3713, Jun. 2023.
- [15] M. Arvinte and J. I. Tamir, “Score-based generative models for robust channel estimation,” *2022 IEEE Wireless Communications and Networking Conference (WCNC)*, Austin, TX, USA, 2022, pp. 453–458.
- [16] X. Niu, X. Wang, D. Gündüz, B. Bai, W. Chen, and G. Zhou, “A hybrid wireless image transmission scheme with diffusion,” *2023 IEEE 24th International Workshop on Signal Processing Advances in Wireless Communications (SPAWC)*, Shanghai, China, 2023, pp. 86–90.
- [17] J. Chen, D. You, D. Gündüz, and P. L. Dragotti, “CommIN: Semantic image communications as an inverse problem with INN-guided diffusion models,” *2024 IEEE International Conference on Acoustics, Speech and Signal Processing (ICASSP)*, Seoul, Korea, Republic of, 2024, pp. 6675–6679.
- [18] F. A. Aoudia and J. Hoydis, “Model-free training of end-to-end communication systems,” *IEEE Journal on Selected Areas in Communications*, vol. 37, no. 11, pp. 2503–2516, Nov. 2019.
- [19] J. Sohl-Dickstein, E. Weiss, N. Maheswaranathan, and S. Ganguli, “Deep unsupervised learning using nonequilibrium thermodynamics,” *Proceedings of the 32nd International Conference on Machine Learning*, Francis R. Bach and David M. Blei (Eds.), Lille, France, Jul. 2015, vol. 37, pp. 2256–2265.
- [20] D. P. Kingma, T. Salimans, and M. Welling “Variational dropout and the local reparameterization trick,” *Advances in Neural Information Processing Systems (NIPS 2015)*, vol. 28, 2015.
- [21] E. Björnson, J. Hoydis, M. Kountouris, and M. Debbah, “Massive MIMO systems with non-ideal hardware: Energy efficiency, estimation, and capacity limits,” *IEEE Transactions on Information Theory*, vol. 60, no. 11, pp. 7112–7139, Nov. 2014.
- [22] J. Hoydis, S. Cammerer, F. A. Aoudia, A. Vem, N. Binder, G. Marcus, and A. Keller, “Sionna: An open-source library for next-generation physical layer research,” *arXiv preprint arXiv:2203.11854*, Mar. 2023.
- [23] Y. -J. Lu, Z. -Q. Wang, S. Watanabe, A. Richard, C. Yu, and Y. Tsao, “Conditional diffusion probabilistic model for speech enhancement,” *2022 IEEE International Conference on Acoustics, Speech and Signal Processing (ICASSP)*, Singapore, Singapore, 2022, pp. 7402–7406.
- [24] S. A. Ameli Kalkhoran, M. Letafati, E. Erdemir, B. H. Khalaj, H. Behroozi, and D. Gündüz, “Secure deep-JSCC against multiple eavesdroppers,” *2023 IEEE Global Communications Conference*, Kuala Lumpur, Malaysia, 2023, pp. 3433–3438.
- [25] L. Deng, “The MNIST database of handwritten digit images for machine learning research [Best of the Web],” *IEEE Signal Processing Magazine*, vol. 29, no. 6, pp. 141–142, Nov. 2012, doi: 10.1109/MSP.2012.2211477.
- [26] O. Ronneberger, P. Fischer, and T. Brox, “U-Net: Convolutional networks for biomedical image segmentation,” *International Conference on Medical Image Computing and Computer-Assisted Intervention*, pp. 234–241. Springer, 2015.
- [27] Y. Song and S. Ermon, “Improved techniques for training score-based generative models,” *Advances in Neural Information Processing Systems 33 (NeurIPS 2020)*, Dec. 2020.
- [28] A. Vahdat and K. Kreis (2022, Apr. 26). “Improving Diffusion Models as an Alternative To GANs,” *NVIDIA Research*, [Online]. Available: <https://developer.nvidia.com/blog/improving-diffusion-models-as-an-alternative-to-gans-part-2/> [Accessed Oct. 25, 2024]



- [29] T. J. Richardson and R. Urbanke, *Modern Coding Theory*. Cambridge University Press, 2008.
- [30] B. J. Kschischang Frey and H. A. Loeliger, "Factor graphs and the sum-product algorithm," *IEEE Transactions on Information Theory*, vol. 47, no. 2, pp. 498–519, 2001.
- [31] K. He, X. Zhang, S. Ren, and J. Sun, "Deep residual learning for image recognition," in Proc. *IEEE conference on computer vision and pattern recognition*, 2016, pp. 770–778.